

# Measurements of Ion Stopping about the Bragg Peak In High-Energy-Density Plasmas

J. A. Frenje<sup>1</sup>, P. E. Grabowski<sup>2</sup>, C. K. Li<sup>1</sup>, F. H. Séguin<sup>1</sup>, A. B. Zylstra<sup>1,\*</sup>, M. Gatu Johnson<sup>1</sup>, R. D. Petraso<sup>1</sup>, V. Yu Glebov<sup>3</sup> and T. C. Sangster<sup>3</sup>

<sup>1</sup>*Plasma Science and Fusion Center, Massachusetts Institute of Technology, Cambridge, Massachusetts 02139, USA*

<sup>2</sup>*Department of Chemistry, University of California Irvine, Irvine, California 92697 USA*

<sup>3</sup>*Laboratory for Laser Energetics, University of Rochester, Rochester, New York 14623, USA*

For the first time, quantitative measurements of ion stopping at energies about the Bragg peak (or peak ion stopping, which occurs at an ion velocity comparable to the average thermal electron velocity), and its dependence on electron temperature ( $T_e$ ) and electron number density ( $n_e$ ) in the range of 0.5 – 4.0 keV and  $3 \times 10^{22} – 3 \times 10^{23} \text{ cm}^{-3}$  have been conducted, respectively. It is experimentally demonstrated that the position and amplitude of the Bragg peak varies strongly with  $T_e$  with  $n_e$ . The importance of including quantum diffraction is also demonstrated in the stopping-power modeling of High-Energy-Density Plasmas.

**PACS numbers:** 52.25.-b, 52.25.Fi, 52.38.Ph, 52.70.Nc

A fundamental understanding of DT-alpha stopping in High-Energy-Density Plasmas (HEDP) is essential to achieving hot-spot ignition at the National Ignition Facility (NIF) [1]. This requires accurate knowledge about the evolution of plasma conditions and the DT-alpha transport and energy deposition in plasmas for a wide range of electron ( $T_e$ ) and ion temperatures ( $T_i$ ) spanning from tens of eV to tens of keV, and electron number densities ( $n_e$ ) from  $\sim 10^{21}$  to  $\sim 10^{26} \text{ cm}^{-3}$ .

Over the last decades, ion stopping in weakly- to strongly-coupled HEDP has been subject to extensive analytical and numerical studies [2-10], but only a limited set of experimental data exists to validate these theories. Most previous experiments also used only one type of ion with relatively high initial energy, in plasmas with  $n_e < 10^{23} \text{ cm}^{-3}$  and  $T_e < 60 \text{ eV}$  [11-21]. In addition, none of these experiments probed the detailed characteristics of the Bragg peak (or peak ion stopping), which occurs at an ion velocity comparable to the average thermal electron velocity. To the best of our knowledge, only one experimental attempt to do this was made by Hicks et al. [22], who measured ion stopping in a plasma with  $T_i$  of  $\sim 5 \text{ keV}$  and  $n_e$  of  $\sim 10^{22} \text{ cm}^{-3}$ . In this experiment, Hicks et al. measured energy loss of the ions produced in the nuclear reactions



where the birth energies shown in the parentheses are for a “zero temperature” plasma [23]. From the observed energy losses of these ions, Hicks et al. were able to describe qualitatively the behavior of the ion stopping for one plasma condition. The work described here makes significant advances over previous experimental efforts, by quantitatively assessing the characteristics of the ion stopping about the Bragg peak for different HEDP conditions. This was done through accurate measurements of energy loss of the four ions, produced in reactions (1) and (2).

The new experiment, carried out at the OMEGA laser [24], involved implosions of eighteen thin  $\text{SiO}_2$  capsules filled with equimolar deuterium- ${}^3\text{He}$  gas. The capsule shells were 850 to 950  $\mu\text{m}$  in diameter, 2.1 to 2.8  $\mu\text{m}$  thick, and had an initial gas-fill pressure ranging from 3 to 27 atm. These capsules were imploded with sixty laser beams that uniformly delivered up to 10.6 kJ to the capsule in a 0.6-ns or 1-ns square pulse, resulting in a laser intensity on capsule up to  $\sim 4 \times 10^{14} \text{ W/cm}^2$  [25]. Table 1 lists the capsule and laser parameters, along with some measured and inferred implosion parameters for a subset of four implosions discussed in detail in this paper.

To determine the energy lost by the four ions as they traversed the plasma, energy spectra of the emitted ions were measured simultaneously with two magnet-based charged-particle spectrometers (CPS1 and CPS2) [28]. Six Wedge-Range-Filter (WRF) proton spectrometers [28] positioned at various locations around the implosion were also used to measure  $\text{D}^3\text{He}$ -proton spectrum. An example of spectra measured with CPS2 for two implosions, with similar total areal-density ( $\rho R$ ) values [29], where most of the energy loss took place in the cold remaining glass-shell (blue spectra) and in the hot  $\text{D}^3\text{He}$  fuel (red spectra) is shown in FIG. 1. By contrasting the measured mean energies, indicated in FIG. 1, to the birth energies of the ions (temperature corrected), an average energy loss ( $-\Delta E_i$ ) was determined and used to assess the plasma-stopping power. As shown in FIG. 1, the DD-tritons, DD-protons and  $\text{D}^3\text{He}$ -alphas display significantly larger  $-\Delta E_i$  in the cold plasma than in the hot plasma. The  $\text{D}^3\text{He}$ -protons, on the other hand, exhibit a similar  $-\Delta E_i$  in these two plasmas, as they probe plasma stopping at velocities well above the Bragg peak. These differences are discussed in detail below. In addition, the uncertainties associated with the measured mean energies shown in FIG. 1, are mainly due to the spectrometer energy-calibration error (in some cases statistics also affects the uncertainties), which dictates the total uncertainty in the determined  $-\Delta E_i$ .

To make use of the measured  $-\Delta E_i$  and assess the plasma stopping power, it is necessary to

determine the HEDP conditions through which the ions traversed. For each implosion, a  $T_i$  and a DD yield were measured from the Doppler broadened neutron-Time-of-Flight (nTOF) signal [30]. A second measurement of  $T_i$  was obtained for each implosion from the DD- $D^3He$  yield ratio, and the  $T_i$  values and uncertainties used in this paper are weighted averages of these two measurements.  $D^3He$  and DD burn profiles were measured with the Proton Core Imaging System (PCIS) [31], and the  $D^3He$  and DD burn duration was measured with the Particle Temporal Diagnostic (PTD) and Neutron Temporal Diagnostic (NTD) [32-33], respectively. A secondary-neutron yield relative to the primary neutron yield ( $Y_{2n}/Y_{1n}$ ) was also measured for a  $D^3He$ -fuel  $\rho R$  determination [34].

For the eighteen implosions, the measured DD and  $D^3He$  yield ranged from  $2.0 \times 10^9$  to  $1.2 \times 10^{10}$  and from  $1.2 \times 10^8$  to  $1.3 \times 10^{10}$ , respectively;  $T_i$  ranged from 2.7 keV to 11.6 keV; the DD- and  $D^3He$ -burn duration both ranged from 150 to 180 ps; and the measured size of the DD- and  $D^3He$ -burn profiles ranged from  $\sim 45$  to  $\sim 100 \mu\text{m}$  and  $\sim 30$  to  $\sim 60 \mu\text{m}$  (radius at 1/e relative to the peak intensity), respectively. Using 1-D modeling of the implosion, involving a parabolic temperature profile and constant  $D^3He$ -fuel density, a good match to these nuclear observables was found for average ion-number densities ( $n_i$ ) ranging of  $2 \times 10^{22} - 2 \times 10^{23} \text{ cm}^{-3}$  ( $n_e \approx 1.5 n_i$  for these  $D^3He$  plasmas).  $T_e$  could not be measured directly in these experiments, but was qualitatively and independently assessed from the  $n_e$ ,  $n_i$ ,  $T_i$  and burn-duration data. A  $Y_{2n}/Y_{1n}$  ratio up to  $(3.96 \pm 0.17) \times 10^{-4}$  was measured, which corresponds to a  $D^3He$  fuel  $\rho R$  up to 7 mg/cm<sup>2</sup>. The  $\rho R$  of the remaining unablated shell was determined from benchmarked 1-D simulations [35], which indicate that the fuel  $\rho R$  is about an order of magnitude larger than the remaining-shell  $\rho R$  for the implosions with a 1-ns laser-pulse drive, while the remaining-shell  $\rho R$  dominates the  $D^3He$ -fuel  $\rho R$  for the implosions with a 0.4-ns laser-pulse. As a consequence, the ion energy loss is mainly taking place in the  $D^3He$ -fuel in the 1-ns implosions and in the remaining unablated shell in the 0.4-ns implosions.

Although the HEDP conditions have been characterized, the information is not sufficient for distinguishing state-of-art plasma-stopping-power theories at  $v_i \sim v_{th}$ , i.e., at the Bragg peak, which is the long-term goal of this effort. For this, we need information on how the spatial profiles of  $n_e$  and  $T_e$  vary in time during the nuclear production period. Instead, our aim is twofold. First, we simply aim to experimentally demonstrate that the amplitude of the position and amplitude of the Bragg peak varies strongly with  $T_e$  with  $n_e$ . Secondly, as the impact parameter of closest approach between the projectile ions and plasma electrons can be smaller than the de Broglie wavelength, we also aim to demonstrate the importance of including quantum diffraction in the stopping-power modeling of the ion-energy-loss at these HEDP conditions.

The Brown-Preston-Singleton (BPS) [4] and the Li-Petrasso (LP) stopping [5] formalisms were used to model the data. The BPS formalism includes a Coulomb logarithm in the weakly coupled limit, which is derived using the dimensional continuation method, and the LP stopping formalism is derived from a Fokker-

Planck collision operator that uses an ad hoc Coulomb logarithm. Although these formalisms have limitations, they are used in this work to explore if the dominant physics is captured. FIG. 2 illustrates the BPS (black solid) and LP (green solid) proton stopping curves, given in keV/(mg/cm<sup>2</sup>), for a hypothetical uniform plasma that is representative for the HEDP conditions in these experiments. At  $v_i > v_{th}$ , the BPS and LP formalisms predict similar charged-particle stopping, while there is  $\sim 20\%$  at  $v_i \sim v_{th}$ . The BPS quantum (dotted black) and the BPS classical (dashed black) are also shown to illustrate their significance. For this plasma condition, the quantum reduction to the classical ion stopping is  $\sim 25\text{--}30\%$ .

An effective way to evaluate the measured  $-\Delta E_i$  of ions with different birth energy ( $E_i$ ), charge ( $Z_i$ ) and mass ( $A_i$ ) is to show the dependency between  $-\Delta E_i/Z_i^2$  and  $E_i/A_i$ . Presenting the data in this form, the ion energy loss is almost exclusively a function of  $v_i$  (any explicit dependence on  $A_i$  and  $Z_i$  is small and restricted to the slowly varying Coulomb logarithm) and can easily be analyzed using a plasma stopping power model. FIGS. 3a and 3b illustrate the  $-\Delta E_i/Z_i^2$  vs  $E_i/A_i$  dependence on  $T_e$ . This data set was directly determined from the low-temperature and high-temperature data shown in FIG. 1. The black (green) curves are the BPS (LP) modeled fits to the data. These curves were obtained by integrating the plasma-stopping-power functions over assumed values of  $T_e$  and  $\rho R$ , which were varied until best fits to the data were obtained. Clearly, these experimental results demonstrate that the plasma-stopping-power function varies with  $T_e$  in the framework of the BPS and LP formalisms. At  $T_e$  of  $\sim 0.6$  keV ( $\Gamma = 1.4\%$ ; see Table 1), the effective proton Bragg peak is 220 keV/(mg/cm<sup>2</sup>), which is reduced to 40 keV per mg/cm<sup>2</sup> for a  $T_e$  of  $\sim 4$  keV ( $\Gamma = 0.3\%$ ; see Table 1). This reduction is caused by the fact that  $v_i \sim v_{th}$  for the DD-tritons, D<sup>3</sup>He-alphas and DD-protons in the low-temperature case, while  $v_i < v_{th}$  for these ions in the high-temperature case. This agrees with theories in which the Bragg peak scales with  $1/T_e$ . The average energy loss of the D<sup>3</sup>He-protons is, on the other hand, unaffected by an increasing  $T_e$  because  $v_i > v_{th}$ . In contrast, the two data sets shown in FIGS. 4a and 4b illustrate the  $-\Delta E_i/Z_i^2$  vs  $E_i/A_i$  dependence on  $\rho R$  (or  $n_e$  [29]), which indicates that the D<sup>3</sup>He-proton energy loss increases with increasing  $\rho R$  with  $\sim 40$  keV/(mg/cm<sup>2</sup>) differential.

To fully constrain and validate the stopping power formalisms used to model this type of data, an independent measurement of  $T_e$  and  $\rho R$  (or  $n_e$ ) must be made. In these experiments,  $T_e$  could not be measured directly, but a D<sup>3</sup>He fuel  $\rho R$  was determined from the measured  $Y_{2n}/Y_{In}$  ratio for most implosions. In the case of the high- $\rho R$  implosion shown in FIG. 4b (implosion 27814), a  $Y_{2n}/Y_{In}$  ratio of  $(3.96 \pm 0.17) \times 10^{-4}$  was measured, which corresponds to a D<sup>3</sup>He-fuel  $\rho R$  of  $7.1 \pm 0.3$  mg/cm<sup>2</sup>. According to benchmarked 1D-implosion simulations, this represents 88% of the total  $\rho R$  of  $8.1 \pm 0.3$  mg/cm<sup>2</sup> (D<sup>3</sup>He fuel  $\rho R$  + glass-shell  $\rho R$ ). FIG. 5 shows the high- $\rho R$  implosion data contrasted to BPS and LP modeling that use the fixed  $\rho R$  value of 8.1 mg/cm<sup>2</sup> and a varying  $T_e$  to minimize the reduced  $\chi^2$ . For comparison, BPS

modeling of the data was also done when the quantum component was switched off. Here, the inferred  $T_e$  is dictated mainly by the energy loss of the DD-tritons, D<sup>3</sup>He-alphas and DD-protons because  $v_{th}$  is similar to the velocities of these ions. In contrast, the energy loss of the D<sup>3</sup>He-protons is insensitive to  $T_e$  for these plasma conditions, but linearly proportional to the  $\rho R$ . As a consequence, the classical modeling can be shown experimentally inconsistent with the  $\rho R$  measurement and its uncertainty alone. We find that classical BPS theory over-predicts the ion stopping, indicating the importance of including quantum diffraction in the plasma-stopping-power modeling of the energy-loss data in these weakly-coupled HEDP. In addition, the full BPS and LP formalisms agree with the data for  $v_i > v_{th}$ , while there are some discrepancies for  $v_i \sim v_{th}$ . However, as the plasma stopping power at  $v_i \sim v_{th}$  is highly sensitive to  $T_e$ , and that a direct measurement of  $T_e$  is lacking, any definite conclusions about the modeling of the data at  $v_i \sim v_{th}$  cannot be made with this data set. To further validate and elucidate stopping-power formalisms at the Bragg peak, measurements of  $n_e(r, t)$  and  $T_e(r, t)$  will be conducted in future experiments using x-ray imaging spectroscopy of a dopant such as argon in the D<sup>3</sup>He fuel [37].

In summary, ion stopping about the Bragg peak and its dependence on plasma conditions has been measured for the first time in HEDP. The experimental data generally support the predictions of the BPS and LP formalisms, demonstrating the plasma stopping power variation with  $T_e$  and  $\rho R$  (or  $n_e$ ). It has also been experimentally demonstrated that classical stopping over-predicts the ion stopping, which is to be expected as it does not include quantum diffraction. The BPS and LP formalisms, with 25-30% quantum reduction to the ion stopping, agree with the data for  $v_i > v_{th}$ . There are some differences at  $v_i \sim v_{th}$ , but the current data set cannot distinguish between them. These experimental results represent the first sensitive tests of plasma-stopping-power theories about the Bragg peak, an important first step towards accurately validating state-of-art plasma-stopping-power theories, which use microscopically-based quantum approaches that overcome the limitations of the BPS and LP models used in this work. In addition, the long-term goal with this effort is to establish a fundamental understanding of DT-alpha stopping in HEDP, which is a prerequisite for achieving hot-spot ignition at the NIF.

The work described herein was performed in part at the LLE National Laser User's Facility (NLUF), and was supported in part by US DOE (Grant No. DE-FG03- 03SF22691), LLNL (subcontract Grant No. B504974) and LLE (subcontract Grant No. 412160-001G). In addition, Grabowski acknowledges support from the Laboratory Directed Research and Development Program at LLNL under tracking code No. 12-SI-005.

\* Currently at Los Alamos National Laboratory, Los Alamos, New Mexico 87545, USA.

- [1] G.H. Miller et al. “The National Ignition Facility: enabling fusion ignition for the 21st century”, Nucl. Fusion 44, S228 (2004).
- [2] T.A. Mehlhorn “A finite material temperature model for ion energy deposition in ion driven inertial confinement fusion targets”, J. Appl. Phys. 52, 6522 (1981).
- [3] T. Peter et al. “Energy loss of heavy ions in dense plasma. I. Linear and nonlinear Vlasov theory for the stopping power”, Phys. Rev. A 43, 1998 (1991).
- [4] L.S. Brown et al. “Charged particle motion in a highly ionized plasma”, Phys. Reports 410, 237 (2005).
- [5] C.K. Li and R.D Petrasso, “Charged-particle stopping powers in Inertial Confinement Fusion plasmas”, Phys. Rev. Lett. 70, 3059 (1993). C.K. Li and R. D. Petrasso, Erratum: Charged-particle stopping powers in Inertial Confinement Fusion Plasmas [Phys. Rev. Lett. 70, 3059 (1993)]”, Phys. Rev. Lett. 114, 199901 (2015).
- [6] D.O. Gericke et al. “Stopping power of a quantum plasma – T-matrix approximation and dynamical screening”, Phys. Letters A 222, 241 (1996).
- [7] G. Zwicknagel et al. “Stopping of heavy ions in plasmas at strong coupling”, Phys. Reports 209, 117 (1999).
- [8] G. Maynard et al. “Energy loss and straggling of ions with any velocity in dense plasmas at any temperature”, Phys. Rev. A 26, 665 (1982).
- [9] G. Maynard et al. “Born random phase approximation for ion stopping in an arbitrarily degenerate electron fluid”, J. Physique 46, 1113 (1985).
- [10] P.E. Grabowski et al. “Molecular dynamics simulations of classical stopping power”, Phys. Rev. Lett. 111, 215002 (2013).
- [11] F.C. Young et al. “Measurements of enhanced stopping of 1-MeV deuterons in target-ablation plasmas”, Phys. Rev. Lett. 49, 549 (1982).
- [12] D.H.H. Hoffmann et al. “Energy loss of heavy ions in a plasma target”, Phys. Rev. A 42, 2313 (1990).
- [13] G. Belyaev et al. “Measurement of the Coulomb energy loss by fast protons in a plasma target”, Phys. Rev. E 53, 2701 (1996).
- [14] C. Stöckl et al. “Experiments on the interaction of heavy-ion beams with dense plasmas”, Fusion Tec. 31, 169 (1997).
- [15] C. Stöckl et al. “Experiments on the interaction of ions with dense plasma at GSI-Darmstadt”, Nucl. Instrum. Meth. A415, 558 (1998).
- [16] M. Roth et al. “Energy loss of heavy ions in laser-produced plasmas”, Europhys. Lett., 50, 28 (2000).

- [17] A. Golubev et al. “Experimental investigation of the effective charge state of ions in beam-plasma interaction”, Nucl. Instrum. Meth. A464, 247 (2001).
- [18] K. Shibata et al. “A TOF system to measure the energy loss of low energy ions in a hot dense plasma”, Nucl. Instrum. Meth. B161, 106 (2000).
- [19] A. B. Zylstra et al. “Measurement of charged-particle stopping in Warm Dense Plasma”, Phys. Rev. Lett. 114, 215002 (2015).
- [20] F.R. Graziani et al. “Large-scale molecular dynamics simulations of dense plasmas: The Cimarron Project”, High. En. Dens. Phys. 8, 105 (2012).
- [21] J. Jacoby et al. “Stopping of heavy ions in a hydrogen plasma”, Phys. Rev. Lett. 74, 1550 (1995).
- [22] D.G. Hicks et al. “Charged-particle acceleration and energy loss in laser-produced plasmas”, Phys. Plasmas 7, 5106 (2000).
- [23] For a finite temperature, the mean energy of the fusion products is slightly upshifted by a few tens of keV [22].
- [24] T.R. Boehly et al. “Initial performance results of the OMEGA laser system”, Opt. Commun. 133, 495 (1997).
- [25] For these laser and capsule conditions, it has been demonstrated that capsule charging and any energy upshifts of the produced ions are insignificant and thus have no impact on these energy-loss measurements [26]. This is critical when equating a measured energy loss to plasma stopping.
- [26] N. Sinenian et al. “An empirical target discharging model relevant to hot-electron preheat in direct-drive implosions on OMEGA”, Plasma Phys. Control. Fusion 55, 045001 (2013).
- [27] For the plasma degeneracy parameter ( $\theta$ ) shown in Table 1, we used the standard definition of  $k_B T_e / E_F$ , where  $k_B$  is the Boltzmann’s constant and  $E_F$  is the Fermi energy.
- [28] F.H. Séguin et al. “Spectrometry of charged particle from inertial-confinement-fusion plasmas”, Rev. Sci. Instrum. 74, 975 (2003).
- [29] For these low-convergence implosion, which are 1D in nature, the ion-number density ( $n_i$ ) in the D<sup>3</sup>He fuel scales with  $\rho R$  as  $n_i \sim \rho R^{1.5}$ . This means that the electron number density in the clean D<sup>3</sup>He fuel scales with  $\rho R$  as  $n_e \sim 1.5 \rho R^{1.5}$ .
- [30] V. Yu Glebov et al. “Prototypes of National Ignition Facility neutron time-of-flight detectors tested on OMEGA”, Rev. Sci. Instrum. 75, 3559 (2004).
- [31] F.H. Séguin et al. “D<sup>3</sup>He-proton emission imaging for inertial-confinement-fusion experiments”, Rev. Sci. Instrum. 75, 3520 (2004).
- [32] J.A. Frenje et al. “Measuring shock-bang timing and  $\rho R$  evolution of D<sup>3</sup>He implosions at OMEGA”, Phys. Plasmas 11, 2798 (2004).

- [33] C. Stoeckl et al. “Ten-inch manipulator-based neutron temporal diagnostic for cryogenic experiments on OMEGA”, *Rev. Sci. Instrum.* 74, 1713 (2003).
- [34] M.D. Cable et al. “Neutron spectra from inertial confinement fusion targets for measurement of fuel areal density and charged particle stopping powers”, *J. Appl. Phys.* 62, 2233 (1987).
- [35] J.T. Larsen et al. “Hyades – A plasma hydrodynamics code for dense plasma studies”, *J. Quant. Spec. Rad. Trans.*, 51, 179 (1994).
- [36] R. Andrae et al., “Dos and don’ts of reduced chi-squared”, arXiv:1012.3754v1, Dec 2010.
- [37] T. Nagayama et al. “Direct asymmetry measurement of temperature and density spatial distributions in inertial confinement fusion plasmas from pinhole space-resolved spectra”, *Phys. Plasmas* 21, 050702 (2014).

TABLE 1. Capsule and laser parameters for four selected implosions, and measured DD burned-averaged  $T_i$  and determined key implosion parameters [ $n_i$ ,  $T_e$ ,  $n_e$  ( $n_e \approx 1.5n_i$ ), plasma-coupling parameter ( $\Gamma$ ), degeneracy parameter ( $\theta$ ) [27] and total  $\rho R$ , for the region where the energy loss mainly occurred]. For implosion 29828, the energy loss took place mainly in the colder glass-shell plasma, while for the other implosions, the energy loss took place mainly in the hotter D<sup>3</sup>He plasma.

Shot	Capsule	Laser pulse	Laser energy	$T_i$	$n_i$	$T_e$	$n_e$	$\Gamma$	$\theta$	Total	$\rho R$
			[kJ]	[keV]	[cm <sup>-3</sup> ]	[keV]	[cm <sup>-3</sup> ]	[%]			[mg/cm <sup>2</sup> ]
27814	D <sup>3</sup> He(18atm)SiO <sub>2</sub> [2.3μm]OD[948μm]	1-ns square	8.4	3.7	2×10 <sup>23</sup>	1.8	3×10 <sup>23</sup>	0.9	110	8.1	
29828	D <sup>3</sup> He(18atm)SiO <sub>2</sub> [2.6μm]OD[917μm]	0.4-ns Gaussian	9.4	6.7	3×10 <sup>22</sup>	0.6	5×10 <sup>22</sup>	1.4	120	2.0	
43233	D <sup>3</sup> He(18atm)SiO <sub>2</sub> [2.5μm]OD[855μm]	1-ns square	10.6	11.6	5×10 <sup>22</sup>	3.9	8×10 <sup>22</sup>	0.3	580	3.5	
43235	D <sup>3</sup> He(18atm)SiO <sub>2</sub> [2.5μm]OD[854μm]	1-ns square	9.9	10.1	2×10 <sup>22</sup>	2.1	3×10 <sup>22</sup>	0.3	600	1.4	

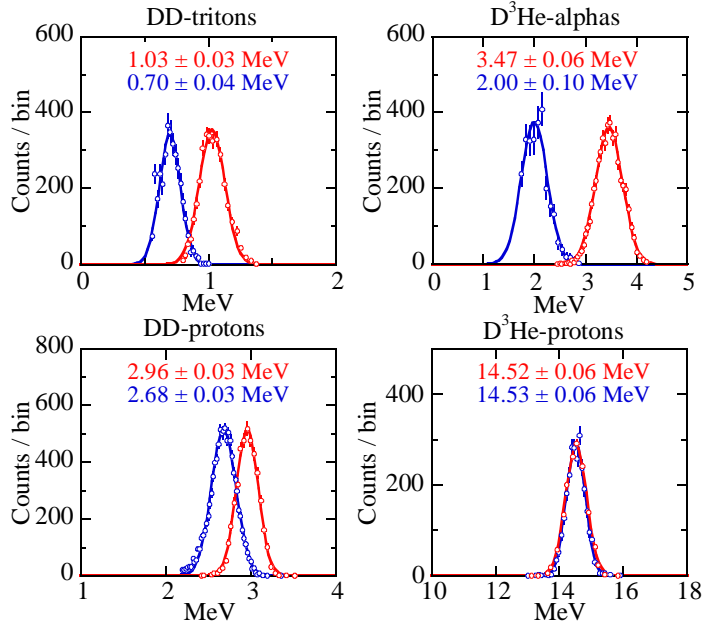


FIG. 1 (color). CPS2-measured spectra of DD-tritons, D<sup>3</sup>He-alphas, DD-protons and D<sup>3</sup>He-protons produced in implosions 29828 (blue) and 43233 (red). These experiments were designed to generate similar total  $\rho R$  values but to have most of the ion energy loss taking place in the cold remaining shell for implosion 29828 (blue spectra) and in the hot fuel for implosion 43233 (red spectra).

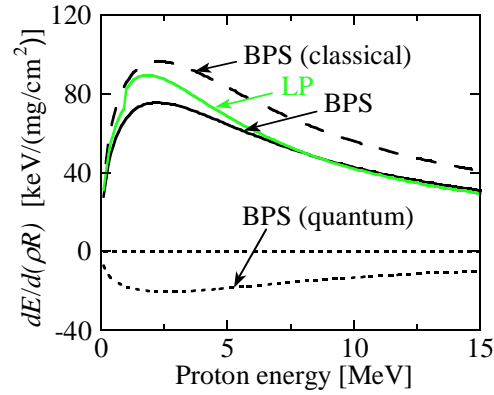


FIG. 2 (color) Brown-Preston-Singleton (BPS) and Li-Petrasso (LP) modeling of proton stopping in a uniform plasma with a  $T_e$  of 1.0 keV and  $n_e$  of  $5 \times 10^{22}$  cm $^{-3}$ . The BPS quantum (dotted black) and BPS classical stopping (dashed black) are also shown.

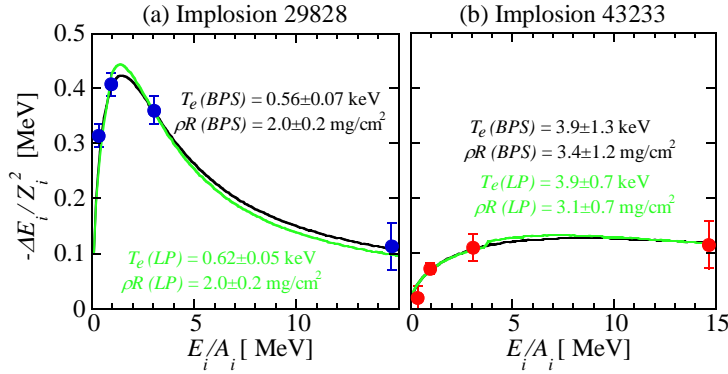


FIG. 3 (color). Stopping-power data illustrating  $T_e$  dependence. Measured and modeled  $-\Delta E_i/Z_i^2$  versus  $E_i/A_i$  for a low-temperature experiment (a), and for a high-temperature experiment (b). Inferred  $\rho R$  was similar in these experiments. The data were determined directly from the spectra shown in FIG. 1. The black (green) curves represent the BPS (LP) modeling. For the low-temperature experiment, the reduced  $\chi^2$  [36] is 2.1 for LP and 0.2 for BPS, and for the high-temperature experiment, the reduced  $\chi^2$  is 1.5 for LP and 1.5 for BPS. The errors on the inferred  $T_e$  and  $\rho R$  values were determined from the reduced  $\chi^2$  fit.

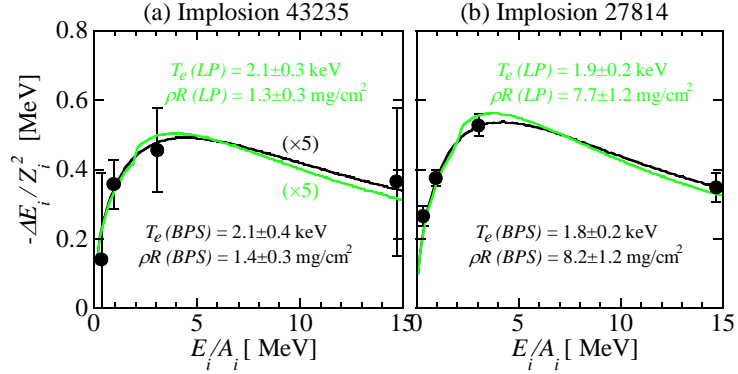


FIG. 4 (color). Stopping-power data illustrating  $\rho R$  (or  $n_e$ ) dependence. Measured and modeled  $-\Delta E_i/Z_i^2$  versus  $E_i/A_i$  for a low- $\rho R$  experiment ( $n_e \sim 3 \times 10^{22} \text{ cm}^{-3}$ ) (a), and for a high- $\rho R$  experiment ( $n_e \sim 3 \times 10^{23} \text{ cm}^{-3}$ ) (b). The experimental and modeled data shown in (a) have been multiplied with a factor of 5 to put the information on the same scale as used in (b). Inferred  $T_e$  was similar in these experiments. The black (green) curves represent the BPS (LP) modeling. For the low- $\rho R$  experiment, the reduced  $\chi^2$  is 0.4 for LP and 0.2 for BPS, and for the high- $\rho R$  experiment, the reduced  $\chi^2$  is 2.3 for LP and 0.7 for BPS. The errors on the inferred  $T_e$  and  $\rho R$  values were determined from the reduced  $\chi^2$  fit.

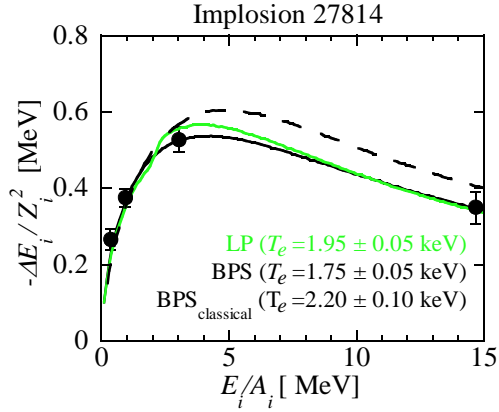


FIG. 5 (color). Measured and modeled  $-\Delta E_i/Z_i^2$  versus  $E_i/A$  for implosion 27814. In the modeling of the energy-loss data,  $\rho R$  was fixed to  $8.1 \text{ mg/cm}^2$  while  $T_e$  was allowed to vary. The reduced  $\chi^2$  is 10.1 for BPS-classical (dashed black), 0.7 for BPS (solid black) and 1.7 for LP (solid green). The errors on the inferred  $T_e$  values were determined from the reduced  $\chi^2$  fit.